Bull. Mater. Sci., Vol. 34, No. 7, December 2011, pp. 1501–1506. © Indian Academy of Sciences.

# Ce-doped LCMO CMR manganites: a consequence of enhanced $T_c$ and $T_{IM}$

**D K MISHRA*, D R SAHU[†], P K MISHRA[††], S K SINGH, B K MOHAPATRA and B K ROUL[§]**

Advanced Materials Technology Department, Institute of Minerals and Materials Technology (CSIR), Bhubaneswar 751 013, India

[†]School of Physics and DST/NRF Centre of Excellence in Strong Materials, University of the Witwatersrand, Private Bag 3, Wits 2050, Johannesburg, South Africa

[††]Technical Physics and Prototype Engineering Division, Bhabha Atomic Research Centre, Mumbai 400 085, India

[§]Institute of Materials Science, Planetarium Building, Bhubaneswar 751 013, India

MS received 30 July 2009; revised 14 February 2011

**Abstract.** **A series of Ce-doped (1–20 mol%) $La_{0.67}Ca_{0.33}MnO_3$ (LCMO) sintered (1400°C) ceramic samples were prepared by the solid-state reaction route. The significant enhancement of metal insulator transition temperature ($T_{IM} \approx 280$ K) and Curie transition temperature ($T_c \approx 270$ K) associated with LCMO system by the addition of 10 mol% of Ce has been observed. Further interesting observation showed that both low ($\approx 1$ mol%) and high ($\geq 15$ and 20 mol%) level of Ce-doping in LCMO reduced the $T_{IM}$ appreciably from 280 K to 220 K, and from 100 to 160 K, respectively exhibiting the signature of a unique spin glass transitions at around 30 K. Structural and spectroscopic studies revealed that unreacted $CeO_2$ and $MnO_2$ phases are found to be present in 1, 15, 20 mol% Ce-doped LCMO samples, which is one of the reasons why they show spin glass transition at low temperature. Our present results on bulk Ce-doped (10 mol%) LCMO are found to be encouraging as far as $T_{IM}$ of epitaxial $La_{0.7}Ce_{0.3}MnO_3$ thin film ($T_{IM} \approx 250$ K) is concerned. This finding suggests that single-phase materials of Ce-doped (10 mol%) LCMO can be prepared with enhanced $T_{IM}$ effectively using solid-state reaction route.**

**Keywords.** **Metal insulator transition; spin glass transition; solid-state reaction route.**

## 1. Introduction

The discovery of colossal magnetoresistance (CMR) phenomenon (Jin *et al* 1994; Rao and Raveau 1995; Rao *et al* 1998a, b; Mitra *et al* 2001;) in perovskite manganites $R_{1-x}A_xMnO_3$ (R = La, Nd, Pr, … and A = Ca, Sr, Ba, …) has already been created significant attention among the researchers due to its various applications (memory cells, magnetic field sensors, hard disk read heads, infrared detectors, microwave active components and miniaturized magnetoelectronic devices). On basis of correlation found in their phase diagram, these systems are considered as spin–lattice coupled system. The phenomenon was originally observed in hole-doped compounds where the rare earth in the insulating parent compound is partially replaced by a divalent cation (such as Ca, Ba, Sr, Pb, etc.) (Mahendiran *et al* 1996; Coey *et al* 1999). This gives rise to a coupling between neighbouring $Mn^{3+}/Mn^{4+}$ pairs via Zener double exchange (Zener 1951) mechanism. But later on, studies on electron (tetravalent or pentavalent ion) doped systems (Mitra *et al* 2001; Roy and Ali 2001; Duan *et al* 2003; Tan *et al* 2003) indicated that CMR behaviour could occur in these systems having mixed valence states of $Mn^{3+}$–$Mn^{2+}$. Among the tetravalent dopant ($Ce^{4+}$, $Te^{4+}$, $Zr^{4+}$ etc.), Ce ion experimentally proved to be very promising (Jo *et al* 2000; Mitra *et al* 2003) for device applications.

The original work of Das and Mandal (1997) for Ce-doped $RMnO_3$ (R = La, Pr and Nd) manganites showed that these compounds are very sensitive to annealing and exhibit ferromagnetic to paramagnetic transition with a resistivity peak near $T_c$ and hence marking a metal–insulator (MI) transition at 250 K for $La_{0.7}Ce_{0.3}MnO_3$ (Mandal and Das 1997). Further studies (Han *et al* 2004) showed that $La_{1-x}Ce_xMnO_3$ systems form as a single phase only in epitaxial thin films (Raychoudhuri *et al* 1999; Mitra *et al* 2001). From photoemission spectroscopy (Han *et al* 2004), it is observed that Ce ion in polycrystalline $La_{0.7}Ce_{0.3}MnO_3$ (LCeMO) bulk samples are mainly in tetravalent (4+) state, which allows the existence of the divalent $Mn^{2+}$ ion, whereas $Ce^{4+}$ valence state and the $Mn^{2+}$ and $Mn^{3+}$ mixed valent states were observed in the thin films of LCeMO (Mitra *et al* 2003; Han *et al* 2004).

*Author for correspondence (dilipiuac@gmail.com)

In another attempt (Raychoudhuri *et al* 1999), a trilayer ferromagnetic tunnel junctions was fabricated using electron (Ce)-doped *n*-type CMR manganites ($T_c$ = 250 K for $La_{0.7}Ce_{0.3}MnO_3$) and a hole (Ca)-doped *p*-type manganites ($T_c$ = 250 K for $La_{0.67}Ca_{0.33}MnO_3$). This *p*–*n* junction showed a large positive tunnelling magnetoresistance (TMR) irrespective of bias voltage, which makes the possibility of the application of *p*–*n* junction and magnetic tunnel junction devices.

An increase of MI transition temperature in electron-doped (Ce) *n*-type CMR is likely to enhance the performance of junction devices with hole-doped *p*-type CMR manganites such as $La_{0.7}Sr_{0.3}MnO_3$ showing $T_{IM} \approx 370$ K. Considering the above observations, many groups have already tried to synthesize Ce-doped and Ce-substituted electron manganites (Gebhardt *et al* 1999; Raychoudhuri *et al* 1999; Mitra *et al* 2001, 2002, 2003; Han *et al* 2004). It is observed that total replacement of Ce in $La_{0.7}Sr_{0.3}MnO_3$ system does not yield encouraging results as the MI transition drops down to 48 K (Gebhardt *et al* 1999). However, no attempt has been made by any research group to enhance the $T_{IM}$ of electron-doped CMR manganites using Ce as an additive. In order to explore the effect of Ce-addition for enhanced $T_{IM}$ and CMR response in LCMO, we have systematically added Ce in different mol%, i.e. ranging from 1–20 mol%. In this paper, we report that there is an optimal limit of the Ce-mol% addition (10 mol%) into LCMO system, which drive the system effectively for achieving higher $T_{IM}$ up to 280 K. However, both lower (< 10 mol%) and higher (> 10–20 mol%) concentrations of Ce mol% lead to the reduction of $T_{IM}$ and the system exhibits signature of a spin glass transition at about 30 K.

## 2. Experimental

Highly pure (99·99%) oxides of La, Ca, Ce and Mn were used as the starting material for preparation of different Ce-added (1–20 mol%) $La_{0.67}Ca_{0.33}MnO_3$ (LCMO) bulk CMR manganite materials. Appropriate stoichiometric compositions of Ce-added LCMO were segregated using a semi-micro electronic balance. Respective oxide powders of each composition were thoroughly mixed and ground repeatedly (four times) before and after calcinations. Well-mixed powders were compacted into circular pellets (10 mm diameter and 3 mm thickness) using high-pressure hydraulic press (10 T/cm$^2$) with suitable polyvinyl alcohol (PVA) as a binder. All pellets were sintered to high density by conventional solid-state sintering route using resistive heating ($Al_2O_3$ tube furnace operated at 1400°C for 10 h). X-ray powder diffractions of all specimens were recorded by Philip Ph-1917 X-ray powder diffractometer using CuK$\alpha$ radiation. The microstructure of the sintered samples was investigated by scanning electron microscopy (SEM) and electron probe microstructure analysis (EPMA) (JEOL-JXA 8100).

A standard four-probe ac technique ($f$ = 17 Hz, $I$ = 1 mA rms) was used to measure the electrical resistance from room temperature down to 50 K. The zero-field cooled (ZFC), field cooled (FC) measurements were carried out from room temperature down to 5 K using a quantum design superconducting quantum interference device (SQUID) magnetometer. Contacts onto the sample for electrical resistance were made by sputter-deposited Ag, which are slowly annealed at 600°C for 1 h for minimization of ohmic contact resistance.

## 3. Results and discussion

X-ray diffraction (XRD) pattern of sintered Ce-added (1, 10, 15 and 20 mol%) LCMO specimens were analysed. Well-defined crystalline XRD peaks are observed and indexed for all samples of Ce-doped LCMO (see, figure S1). It is interesting to note that the number of impurity (unreacted $MnO_2$ and $CeO_2$) peaks are less in 10 mol% of Ce-doped LCMO when compared to 1, 15 and 20 mol% of LCMO. In addition to this, all peaks are distinctly positioned (in 10 mol%) without much background noise. Other Ce-doped LCMO (1, 15 and 20 mol%) do not show this distinct XRD character as compared to 10 mol% of Ce-doped LCMO. This suggests that at this Ce-doping level (10 mol%), the sintered materials are highly crystalline in character. The average particle size of the crystalline particle is calculated using Scherer's formula (Culity 1978), which is of the order of 50 nm. From XRD analysis, unreacted $CeO_2$ and $MnO_2$ phases are seen in case of 1, 15 and 20 mol% of Ce-doped LCMO. Our EPMA studies also showed that unreacted $MnO_2$/$CeO_2$ phases are present in 1, 15 and 20 mol% of Ce-doped LCMO specimen. This situation is very less prominent in case of 10 mole% of Ce-doped LCMO sample. It is important to note here that unreacted $CeO_2$ are seen by other workers (Raychoudhuri *et al* 1999; Mitra *et al* 2001; Srivastava *et al* 2008) in the sample of $La_{0.7}Ce_{0.3}MnO_3$ system. However, thin film of the same composition does not show any unreacted $CeO_2$ (Mitra *et al* 2001) and materials exhibit single phase. Ascribing such structural properties, 10 mol% of Ce-doped LCMO showed higher $T_{IM}$ than that of 1, 15 and 20 mol% of Ce-doped LCMO specimen.

Temperature variation of SQUID magnetization at different low magnetic fields (50 and 100 Oe) for field cooled (FC) and zero field cooled (ZFC) were studied for different Ce-doped LCMO. Low-field (50 and 100 Oe) $M$–$T$ behaviour of 1–20 mol% of Ce-doped LCMO sintered sample for FC and ZFC are shown in figure 1(a–d). Three specific observations pertaining to (a) the transition temperature, (b) splitting of ZFC and FC and (c) signature of spin glass phenomenon are noted in different Ce-doped LCMO. In 1 mol% of Ce-doped LCMO, there is no significant splitting of FC and ZFC line. However,

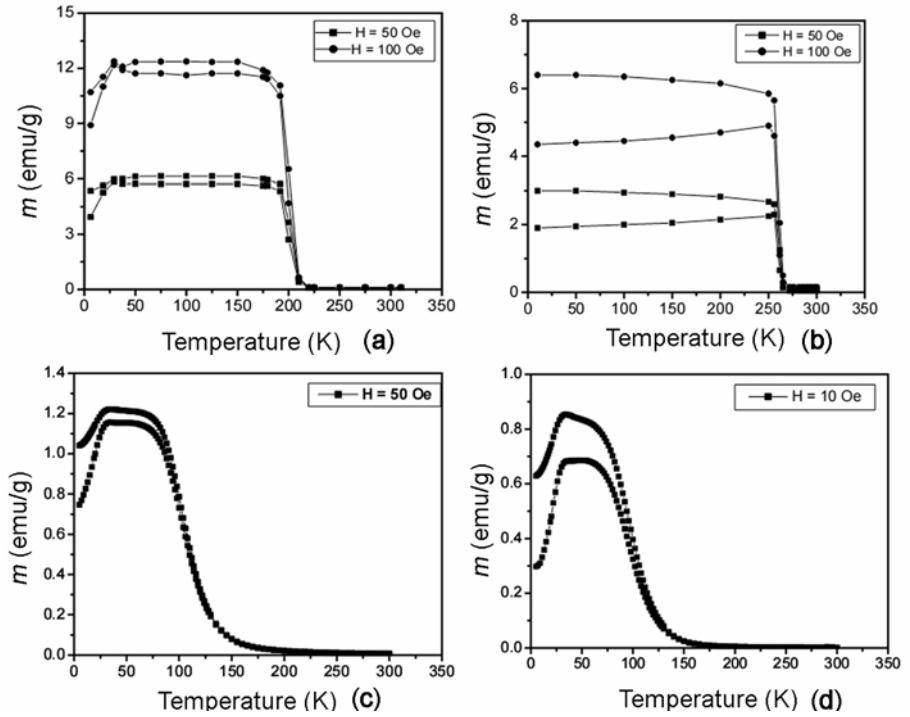


**Figure 1.** Temperature-dependent magnetization of $x$ mol% of Ce-doped $La_{0.67}Ca_{0.33}MnO_3$: (**a**) $x$ = 1 mol%; (**b**) $x$ = 10 mol%; (**c**) $x$ = 15 mol% and (**d**) $x$ = 20 mol%.

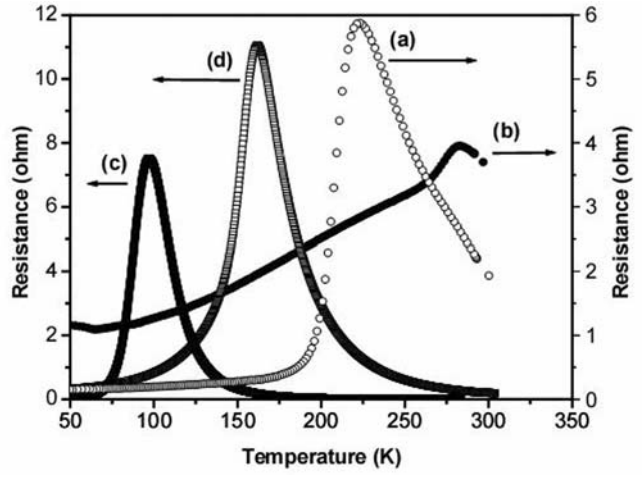


**Figure 2.** Temperature-dependent resistance of $x$ mol% of Ce-doped $La_{0.67}Ca_{0.33}MnO_3$: (a) $x$ = 1 mol%; (b) $x$ = 10 mol%; (c) $x$ = 15 mol% and (d) $x$ = 20 mol%.

two significant transitions are associated at 210 K ($T_c$) and at 30 K (spin glass transition temperature: $T_{SG}$). On the other hand, for 10 mol% Ce-doped LCMO, the $T_c$ is enhanced significantly from 210 to 270 K (figure 1b) without any observable signature of spin glass transition at low temperature. The $T_c$ observed for 10 mol% of Ce-doped ZnO is well above the Curie temperature of LCMO (Rao and Raveau 1995; Pradhan *et al* 2000). In addition to this, significant splitting of FC and ZFC lines are observed (figure 1b) for both 50 and 100 Oe magnetic fields. Higher magnetic field (100 Oe) further enhanced the splitting of FC and ZFC lines appreciably. This kind of behaviour is not seen in other Ce-doped LCMO (1, 15 and 20 mol%) sample. Spin glass transition signature is only observed in case of 1, 15 and 20 mol% Ce-doped LCMO which is almost the same ($\approx$ 30 K) for all Ce-doped LCMO. Typical $M$–$T$ curve of FC and ZFC at low magnetic field for 15 and 20 mol% Ce-doped LCMO sintered samples are shown in figures 1c and d. It is interesting to observe that the addition of Ce in LCMO lowers the transition temperature except in 10 mol% Ce-doped LCMO. The microstructure plays a major role in the enhancement of $T_c$ in 10 mol% Ce-doped LCMO, which is described in terms of our SEM and EPMA results.

It is expected that the addition of Ce in LCMO creates disorder at La site as well as at Mn site due to its existence of multiple valence state +3 and +4 and higher cationic size. Also Ce in the compound leads mixed valence states of +3 and +4 at the La site as well as at the Mn sites for which Mn adopts itself in a multiple valence state of +2, +3 and +4. This results in simultaneous operation of two competing interactions embodying FM double exchange between $Mn^{2+}$–$Mn^{3+}$ and $Mn^{3+}$–$Mn^{4+}$ and antiferromagnetic (AFM) super exchange between $Mn^{2+}$–$Mn^{2+}$ and $Mn^{3+}$–$Mn^{3+}$ (Srivastava *et al* 2008). The competing interaction between double exchange and super exchange interaction determines the nature of magnetic phases and can lead to a canted or helical spin

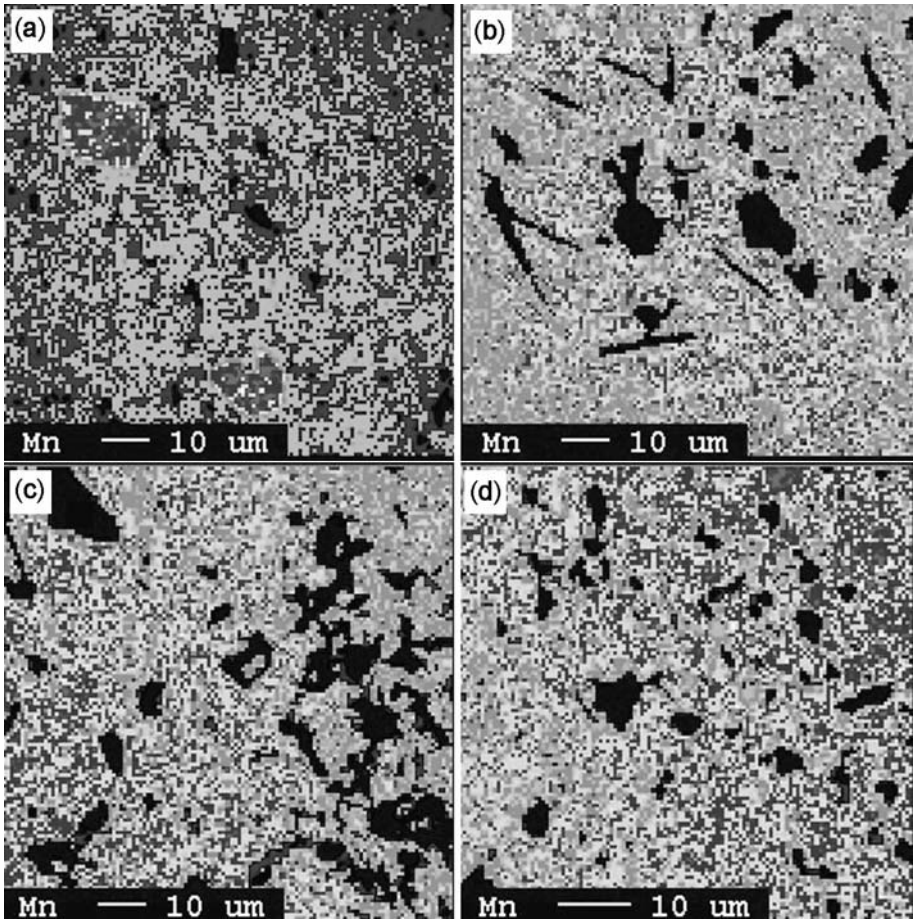


**Figure 3.** EPMA pictures of Mn distribution in $x$ mol% of Ce-doped $La_{0.67}Ca_{0.33}MnO_3$: (**a**) $x = 1$ mol%; (**b**) $x = 10$ mol%, (**c**) $x = 15$ mol% and (**d**) $x = 20$ mol%.

structure, which in turn reduces the Curie transition temperature (de Gennes 1960). Consequently, both double exchange and super exchange interactions compete more strongly and are sufficient enough to suppress the long-range ferromagnetic ordering, giving rise to spatial confined ferromagnetic clusters. These clusters create magnetically disordered state, which favours spin glass-like behaviour at low temperature and lowers the Curie transition temperature (Srivastava *et al* 2008; Siwach *et al* 2009). The mechanism completely supports our result obtained for 1, 15 and 20 mol% Ce-doped LCMO. But in 10 mol% Ce-doped LCMO, microstructure plays the major role for which an enhancement of Curie transition temperature is observed.

To explore further, $R$–$T$ behaviour of all Ce-doped LCMO samples were studied and analysed (figure 2). It is observed (figure 2a, b) that $T_{IM}$ value of 1 mol% (220 K) and 10 mol% (280 K) are always higher than that of the observed $T_c$ (210 and 270 K) value recorded from $M$–$T$ graph. It is interesting to note that the CMR effect in 10 mol% Ce-doped LCMO is drastically reduced as well as the magnetic moment in comparison to 1, 15 and 20 mol% Ce-doped LCMO. On the other hand, $T_{IM}$ values of 15 and 20 mol% of Ce-doped LCMO showed less in comparison to $T_c$ values (175 and 170 K, respectively, for 15 and 20 mol% Ce-doped LCMO). This wide temperature gap between resistance peak and magnetic transition temperature noted for 15 and 20 mol% of Ce-doped LCMO is due to the spin disorder scattering (Das and Mandal 1997). But the role of excess Ce-doping into LCMO may act as an isolated point or clusters of defects between interstitials, which are randomly distributed all over the bulk. Our EPMA result supports this for 15 and 20 mol% Ce-doped LCMO. The flow of the transport current is embedded by these point defects present on the surface and near surface of the bulk. This could be a possible reason for the lowering of $T_{IM}$ as compared to $T_c$ in 15 and 20 mol% Ce-doped LCMO observed by $M$–$T$ plots (shown in figure 1). But the enhancement of $T_c$ and $T_{IM}$ in 10 mol% Ce-doped LCMO can be well understood in terms of grain geometry and interconnectivity.

As the grain geometry and grain boundary junctions in polycrystalline specimen play a crucial role for transport current propagation, SEM studies were carried out to

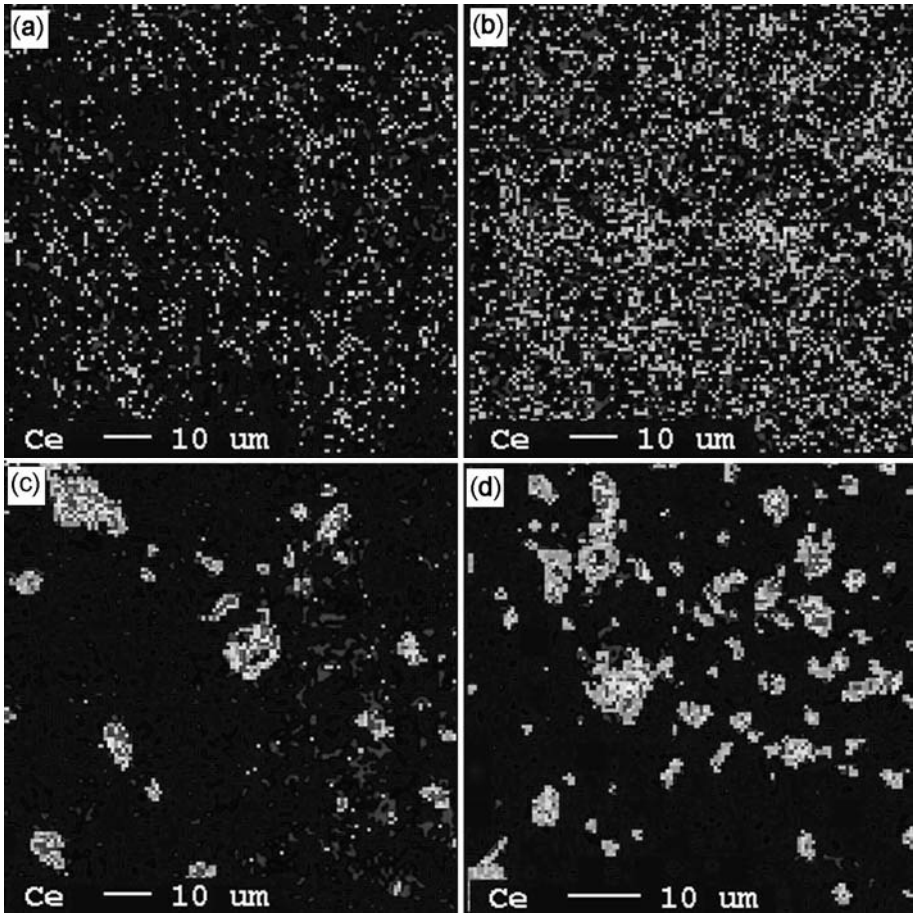


**Figure 4.** EPMA picture of Ce distribution in $x$ mol% of Ce-doped $La_{0.67}Ca_{0.33}MnO_3$: (**a**) $x = 1$ mol%, (**b**) $x = 10$ mol%, (**c**) $x = 15$ mol% and (**d**) $x = 20$ mol%.

understand and correlate the grain boundary junction-dependent transport current propagations. Typical SEM of 1 and 10 mol% of Ce-doped LCMO are given as supporting electronic information (see figure S2). It is noted that there are plenty of unconnected grains associated with the grain growth in 1 mole% of Ce-doped LCMO. However, in 10 mole% doped LCMO (figure S2), the crystalline grain growth are closely packed exhibiting triangular and tetragonal grain boundary junctions. This results in the creation of large number of grain boundary junctions, which is favourable for interconnectivity among the grains. The well-connected grains and the grain boundary junction promote the percolations of transport current observed in electrotransport studies (Pradhan *et al* 2000). The grain growth and grain boundary junctions between the grains enhance spin polarization between the adjacent grains through grain boundary region (Chen and Cheong 1996; Milner *et al* 1996; Mori *et al* 1998; Sun *et al* 1998). As a result, enhancement of $T_{IM}$ up to 280 K is observed in bulk material of 10 mol% Ce-doped LCMO. However, nearly 100% spin polarization in bulk ceramic materials may boost structural MR at $T_c \approx T_{IM}$ in charge transport across the interfaces of the grain boundaries still, which remains an intriguing problem both from technological and scientific points of view.

EPMA of 1, 10, 15 and 20 mol% of Ce-doped LCMO samples were carried out to understand the morphology and the elemental distribution in the bulk of the surface. Figures 3 and 4 present the distribution of Mn and Ce for 1, 10, 15 and 20 mol% of Ce-doped LCMO. It is observed from EPMA that La and Ca are distributed uniformly through out the bulk sample (not shown). However, there is a drastic variation of Ce and Mn distributed as observed in figures 3 and 4. In 1 mol% of Ce-doped LCMO, it is seen (figure 3a) that isolated Mn segregation exists in the bulk surface whereas La, Ca and Ce are homogeneously well distributed. On the other hand, all elements present in 10 mol% of Ce-doped LCMO does not show any isolated segregation of neither Mn nor Ce on the surface of the bulk (figures 3b and 4b). As the Ce-doping concentration increases from 10 to 20 mol%, the unreacted $CeO_2$-isolated segregations are also seen to be increased (figure 4c and d). However, at 20 mol% Ce-doped LCMO (figure 4d), the isolated $CeO_2$ segregation is almost even all over the bulk surface. Considering the appearance of spin glass transition ($T_{SG}$) exactly at 30 K

for 1, 15 and 20 mol% of Ce-doped LCMO, it is expected that presence of either Mn or Ce unreacted oxides may be the reason for it to act as a local short range order point defect site. Further to this, it is also noted from the *M–T* graph (figures 1a, c and d) that $T_{SG}$ ($\approx$ 30 K) does not change in spite of the enhancement of Ce-doping concentration except at 10 mol% Ce-doped LCMO (figure 1b), which may be the intrinsic property of the associated material system (Gebhardt *et al* 1999) with the different concentration of unreacted $MnO_2$ or $CeO_2$ in 1, 15 and 20 mol% of Ce-doped LCMO.

## 4. Conclusions

In conclusion, this paper reports that electron-doped Ce-based $La_{0.67}Ca_{0.33}MnO_3$ bulk materials may be designed to achieve high $T_{IM}$ and $T_c$ close to room temperature. Highly dense and crystalline bulk ceramics of 10 mol% of Ce-doped LCMO can be prepared by solid-state reaction route that exhibits $T_{IM}$ at 280 K without showing the signature of spin glass transition ($T_{SG}$) at low temperature. However, other compositions of Ce-doped (1, 15 and 20 mol%) LCMO showed less $T_{IM}$ and $T_c$ with the appearance of spin glass transition at 30 K. Our studies showed that presence of unreacted and isolated $MnO_2$ or $CeO_2$ may be the possible cause for the appearance of unique spin glass transition at 30 K. Apart from spin disorder scattering, scattering from unreacted and isolated $CeO_2$ and $MnO_2$ may also be the another cause for showing the spin glass transition signature. However, one can confirm this $T_{SG}$ phenomenon by a.c. susceptibility measurement at different frequencies.

## Acknowledgements

One of the authors (DKM) is thankful to Council of Scientific and Industrial Research (CSIR), New Delhi, India for providing financial support for his research work. Authors are thankful to Director, IMMT for providing research support.

## Supporting information available

X-ray diffraction figures and SEM pictures. This material is available free of charge via the internet.

## References

Chen C H and Cheong S W 1996 *Phys. Rev. Lett.* **76** 4042
Coey J, Viret M and Von Molnar S 1999 *Adv. Phys.* **48** 167
Culity B D 1978 *Elements of X-ray diffraction* (New York: Addison-Wesley) p. 278
Das S and Mandal P 1997 *Z. Phys.* **B104** 7
de Gennes P G 1960 *Phys. Rev.* **118** 141
Duan P, Tan G, Dai S, Zhou Y and Chen Z 2003 *J. Phys.: Condens. Matter* **15** 4469
Gebhardt J R, Roy S and Ali N 1999 *J. Appl. Phys.* **85** 5390
Han S W, Kang J S, Kim K H, Wi S H, Mitra C, Raychoudhuri P, Wirth S, Kim K H, Kim B S, Jeong J I, Kwon S K and Min B I 2004 *Phys. Rev.* **B69** 104406
Jin S, Tiefel T H, McCormack M, Fastnacht R A, Ramesh R and Chen L H 1994 *Science* **264** 413
Jo M H, Mathur N D, Evetts J E and Blamire M G 2000 *Appl. Phys. Lett.* **77** 3803
Mahendiran R, Tiwary S K, Raychaudhuri A K, Mahesh R and Rao C N R 1996 *Phys. Rev.* **B54** R9604
Mandal P and Das S 1997 *Phys. Rev.* **B56** 15073
Milner A, Gerber A, Gorisman B, Karpovsky M and Gladkikh A 1996 *Phys. Rev. Lett.* **76** 475
Mitra C, Raychoudhuri P, John J, Dhar S K, Nigam A K and Pinto R 2001 *J. Appl. Phys.* **89** 524
Mitra C, RayChaudhuri P, Kobernik G, Dorr K, Muller K H, Schultz L and Pinto R 2001 *Appl. Phys. Lett.* **79** 2408
Mitra C, Kobernik G, Dorr K, Muller K H, Schultz L, RayChaudhuri P, Pinto R and Wieser E 2002 *J. Appl. Phys.* **91** 7715
Mitra C, RayChaudhuri P, Dorr K, Muller K H, Schultz L, Oppeneer P M and Wirth S 2003 *Phys. Rev. Lett.* **90** 017202 (1–4)
Mitra C *et al* 2003 *Phys. Rev.* **B67** 092404
Mori S, Chen C H and Cheong S W 1998 *Phys. Rev. Lett.* **81** 3972
Pradhan A K, Roul B K, Wen J G, Ren Z F, Muralidhar M, Dutta P, Sahu D R, Mohanty S and Patro P K 2000 *Appl. Phys. Lett.* **76** 763
Rao C N R and Raveau B 1995 *Transition metal oxides* (New York: Wiley VCH Publishers)
Rao C N R, Santhosh P N, Singh R S and Arulraj A 1998a *J. Sol. State Chem.* **135** 169
Rao C N R, Mahesh R, Raychaudhuri A K and Mahendiran R 1998b *J. Phys. Chem. Sol.* **59** 487
Raychoudhuri P, Mukharjee S, Nigam A K, John J, Vaisnav U V, Pinto R and Mandal P 1999 *J. Appl. Phys.* **86** 5718
Roy S and Ali N 2001 *J. Appl. Phys.* **89** 7425
Siwach P K, Srivastava P, Singh H K, Asthana A, Matsui Y, Shripathi T and Srivastava O N 2009 *J. Magn. Magn. Mater.* **321** 1814
Srivastava P, Srivastava O N, Singh H K and Siwach P K 2008 *J. Alloys & Compounds* **459** 61
Sun J R, Rao G H, Shen B G and Wong H K 1998 *Appl. Phys. Lett.* **73** 2998
Tan G T, Dai S Y, Duan P, Lu H B, Zhou Y L and Chen Z H 2003 *Phys. Rev.* **B68** 014426
Zener C 1951 *Phys. Rev.* **82** 403